January 2013

Synthesis and Investigations of type I and II clathrates of Group 14

Michael Blosser
University of South Florida, mblosser1536@gmail.com

Synthesis and Investigations of type I and II clathrates of Group 14

by

Michael C. Blosser

A thesis submitted in partial fulfillment
of the requirements for the degree of
Master of Science
Department of Physics
College of Arts and Sciences
University of South Florida

Major Professor: George S. Nolas, Ph.D.
Lilia Woods, Ph.D.
Pritish Mukherjee, Ph.D.

Date of Approval:
January 23, 2013

Keywords: Material Science, Novel Materials, Novel Synthesis Techniques, Thermoelectrics

Dedication

To my parents, who have supported and been with me every way in my educational endeavors.

Acknowledgments

I would like to thank the Department of Energy for funding this research. I would like to thank Dr.George Nolas for offering me a spot in his lab, for encouraging me and guiding me in my research, and for working with me on any problems that arose. I would like to thank the whole Novel Materials lab, Dr. Yongkwan Dong, Dr. Stevce Stefanoski, Dr. Anuja Datta, and Kaya Wei. I would especially like to thank Dr. Stevce Stefanoski in training me to use all the various research machines and procedures and in conversing with and helping me with our clathrate research. I would like to thank Dr. Matt Beekman, for enlightening conversations and help with my clathrate research. I would like to thank Dr. C. D. Malliakas and Dr. M. G. Kanatzidis from Northwestern University and Fan Sui and Dr. Susan Kauzlarich from UC- Davis for doing the single crystal refinement. I would like to thank Dr. Xianming Han from Butler University for being a great undergraduate advisor and ultimately for encouraging my passion in physics. Finally I wish to express my everlasting gratitude to my family who have been with and supported me through thick and thin and who I love dearly. Thank you all.

Table of Contents

List of Tables

List of Figures

Abstract

Clathrates are a class of new materials that have an open-framework structure that allows guest atoms or molecules to be enclosed inside of their polyhedral framework. Varying the number, weight, and size of the guest species in a particular framework allows one to alter the physical properties of the clathrate. This relationship enables one to further the fundamental understanding of the physics and chemistry of the clathrate structure and use this knowledge to "tune" certain properties. This "tunability" of inorganic clathrates is of great interest as it allows one to optimize their physical properties; making them promising candidates for a range of applications such as thermoelectric, optoelectronic, and superconductivity.

In this study, new synthesis methods of type I and II clathrates of group 14 are introduced, along with two new compositions of type I clathrates. A new synthesis method used to produce single crystal and microcrystalline Na_8Si_{46} and $Na_{24}Si_{136}$ clathrates by the spark plasma sintering technique is introduced. Microcrystalline type I Na_8Si_{46} and type II $Na_{24}Si_{136}$ are also selectively synthesized with no phase impurity of the other type using the low temperature ionic liquid method. In addition, the synthesis of microcrystalline $Na_8Ge_3Si_{38}$ and single crystal $Ba_2Cs_6Ga_8Sn_{38}$ type I clathrates are presented for the first time.

1. Introduction

The word clathrate refers to materials that are able to include "guest species" such as atoms or molecules into their polyhedral framework. The polyhedral framework forms a "cage-like" structure around the "guest species" that allows these "inclusion" atoms or compounds to be varied in their number or type. Changing the number and type of guest species in the host framework allows one to alter the physical properties of the clathrate compounds. The ability to "tune" the physical properties of clathrates holds promise for a variety of applications, from thermoelectrics [1,2,3] , to photovoltaics and optoelectronics [4,5], to potentially ultra-hard materials [6] to magnetic cooling applications [7,8]. This study involves new synthesis methods and new clathrate compounds that furthers the knowledge of the fundamental physics and chemistry involved in the synthesis process of clathrate compounds.

Clathrate hydrates or "gas hydrates" are the first known clathrate compounds where H_2O molecules form the host lattice of the crystal structure in a manner similar to ice and are able to enclose atoms or molecules such as methane and xenon. Currently, there are nine known crystal structures of clathrates [9], with each crystal structure composed of varying face-sharing polyhedral. Not all of the crystal structures have been experimentally produced, with the type I structure being the most frequently published (Figure 1.1).

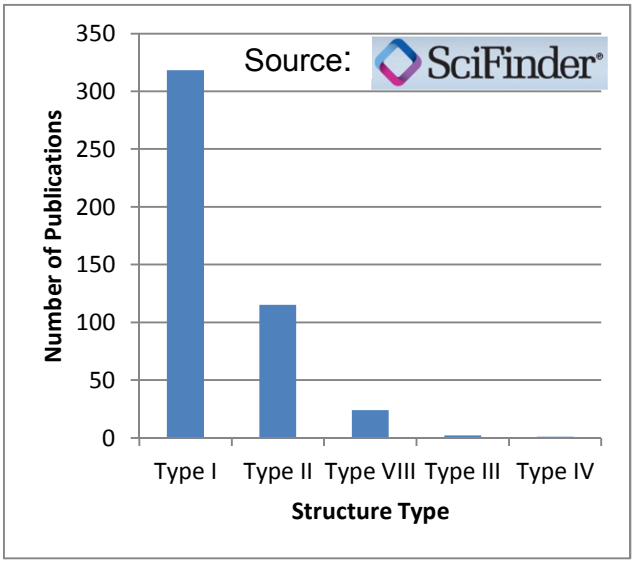

Figure 1.1: Number of clathrate publications by structure type (as of 11/2012).

At this time, most of the known experimentally produced clathrates are composed of the group 14 elements, Si, Ge, and Sn. These group 14 elements form the structural framework of the clathrate with alkali and alkaline earth elements being the most common guest species that reside in the cage-like framework. Group 14 elements have been extensively studied due to their optoelectronic properties and their importance to the field of semiconductor electronics[30,31]. Therefore open-framework materials, such as clathrates, that are composed of group 14 elements are of immense interest as they hold great potential to optimize their physical properties for a variety of applications.

Intermetallic clathrates were first introduced with the type I clathrate, Na_8Si_{46}, being synthesized by Kasper et al. [10] in 1965 with subsequent analysis and characterization of this clathrate undertaken by Cros et al. [11] in 1968. Clathrate research then progressed at a steady rate until the last 15 years which saw a huge uptick in clathrate research and publications (Figure 1.2).

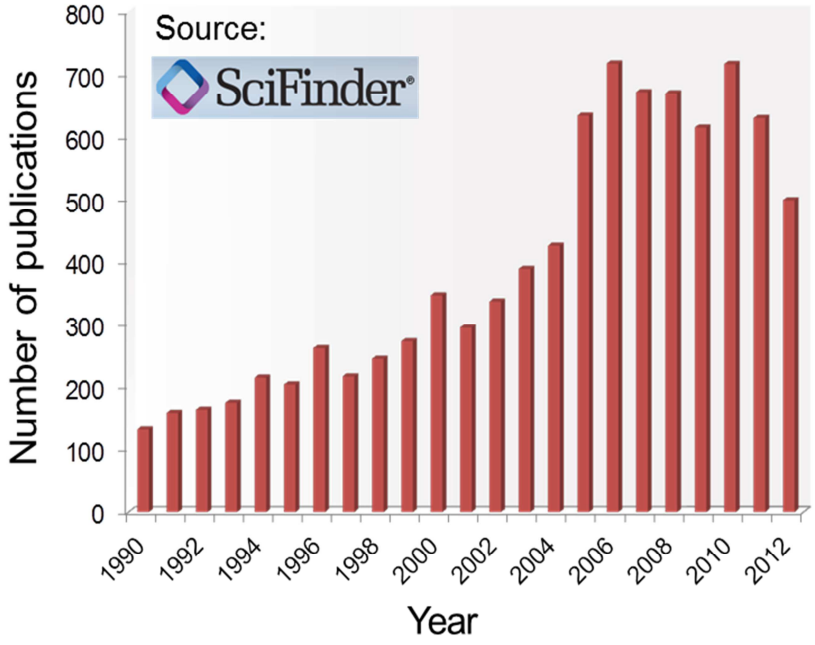

Figure 1.2: Number of clathrate publications by year (as of 11/2012).

From a chemical and physical viewpoint, this huge surge in clathrate research can be largely attributed to the study of the crystal structure of these compounds, their greatly varying physical properties, and how those two qualities are intimately inter-connected. Therefore, being able to understand the fundamental physics and chemistry of these inorganic clathrate compounds is a crucial part in assessing their potential for use in a variety of applications, some of which are mentioned above.

1.1. Crystal structure of type I and II clathrates of group 14

The type I and II clathrates of group 14 are the focus of this research. Their crystal structure consists of face sharing polyhedra with group 14 atoms forming the structural framework with the "guest" consisting of akali metals or akali-earth atoms residing in the polyhedral "cage" created by the framework atoms. The general formula for the crystal

structure of the type I clathrate is $A_8E_{46,}$ with the A consisting of akali metals or akali-earth atoms, and the E consisting of the group 14 elements Si, Ge, or Sn [2,12,13,14]. Type I ternary compounds that have the formula $A_8B_{16}E_{30}$, with B consisting of Zn, Cd, Al, Ga, In, As, Sb, or Bi also exist [15]. In addition, multiple type I clathrates have been synthesized exhibiting a slight variation of these general formulas by varying the host atoms in the framework and by varying the guest atoms in the cages [1].

In most of these compounds, the bonding is considered to adhere to the Zintl concept[16,17], where the electropositive guest atoms donate their valence electrons to the electronegative host atoms, resulting in an electro-neutral compound. These valence electrons are covalently bonded to the host atoms that form the face sharing polyhedra. In the type I clathrate, the host atoms form two types of cages, E_{20} and E_{24}, with the E_{20} being the smaller 20-membered pentagonal dodecahedra formed by twelve pentagonal faces and the E_{24} being the larger 24-membered tetrakaidecahedra formed by twelve pentagonal and two hexagonal faces (Figure 1.3a). The type I crystal structure consists of two E_{20} and six E_{24} cages, with a cubic unit cell and $Pm\bar{3}n$ space group. Three crystallographic sites make up the framework, in the Wyckoff notation, *6c*, *16i*, and *24k*, with the guest atoms residing in the *2a* and *6d* positions inside the E_{20} and E_{24} cages respectively.

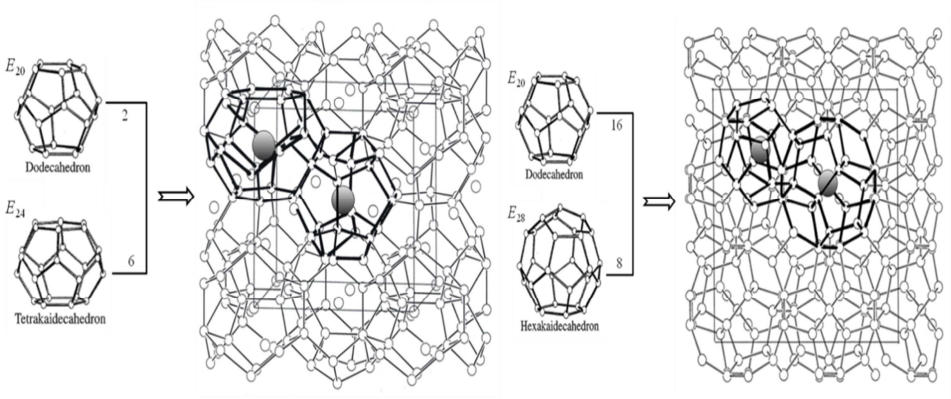

Figure 1.3: a) Crystal structure of the type I clathrate. The cubic unit cell is composed of two pentagonal dodecahedra (E_{20}) and six tetrakaidecahedra (E_{24}).
b) Crystal structure of the type II clathrate. The cubic unit cell is composed of sixteen pentagonal dodecahedra (E_{20}) and eight hexacaidecahedra (E_{28}).
Reprinted with permission from Ref. 1 Copyright [2001], Elsevier Books.

The type II clathrate crystal structure is composed of face sharing polyhedral that create a face centered cubic unit cell of the space group $Fd\bar{3}m$. The type II crystal structure follows the formula $A_{24}E_{136}$ [17,18,19] with E consisting of the group 14 framework atoms and A consisting of the akali-metal or alkaline earth guest atoms. Two types of polyhedra form the unit cell, E_{20} and E_{28}, with E_{20} being the smaller cage formed by 20-membered pentagonal dodecahedra and E_{28} being the larger cage formed by 28-membered hexacaidecahedra (Figure 1.3b). There are 16 E_{20} cages and 8 E_{28} cages in the unit cell of the type II clathrate. The three crystallographic sites (in Wyckoff notation) for the framework atoms are *8a, 32e,* and *96g* while the guest atoms reside in the *8b* and *16*c sites in the polyhedral. The type II clathrates have not been nearly as extensively studied and produced as the type I clathrate, resulting in only 19 known compositions[16,20,21,22].

1.2. Physical Properties of type I and II clathrates of group 14

In order to determine the potential that clathrates hold for applications, one needs to fully understand the physics and chemistry of these compounds. Therefore the characterization of these materials is needed in order to obtain their physical properties and to better understand how their physical properties are related to their crystal structure. Inorganic clathrates have varying electronic and thermal properties that range from semiconductor [3] to metallic[15] behavior.

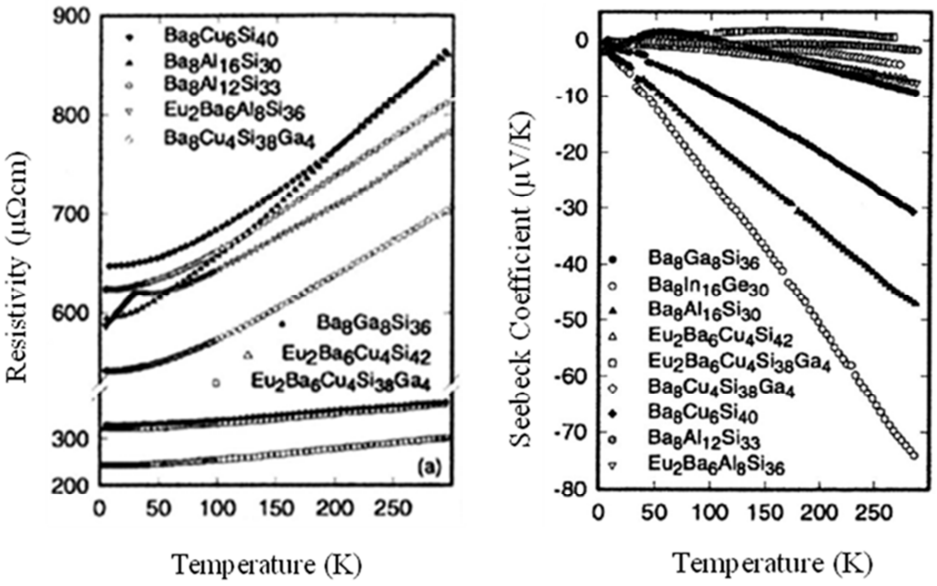

Figure 1.4 : Electrical properties of selected type I clathrates.
Reprinted with permission from Ref. 23. Copyright [2002].
IOP Publishing Limited

A general rigid band model that is typically applied to inorganic clathrates is that the valence electrons from the electropostive guest atoms are donated to the electronegative host framework atoms. If this charge transfer doesn't occur, a partially filled band gap

with a high density of charge carriers results and metallic conduction is expected. Maudryk et al [23] (Figure1.4) and Beekman et al.[24] have characterized type I and II clathrates that exhibit temperature dependent resistivities and low Seebeck coefficients that are typical for metals. Type I clathrates that exhibit semiconducting qualities were also characterized [9]. An important characteristic of these compounds is that one is able to vary the doping level by varying their chemical composition. Semiconducting clathrates of type II have also been synthesized and show great promise for future applications. Type II clathrates are of great interest as they exhibit the ability of removing the guest atoms by the "degas" method [25]. Beekman et al. [24] and Stefanoski et al. [26] used this method to remove the sodium from microcrystalline and single crystal $Na_{24}Si_{136}$ to a final composition of Na_1Si_{136} and $Na_{2.9}Si_{136}$. In doing this, they showed that removing the sodium content from the clathrate changes its electrical properties from metallic to a semiconductor, with a metallic/semiconductor transition occurring at the sodium content of Na~8 (Figure 1.5).

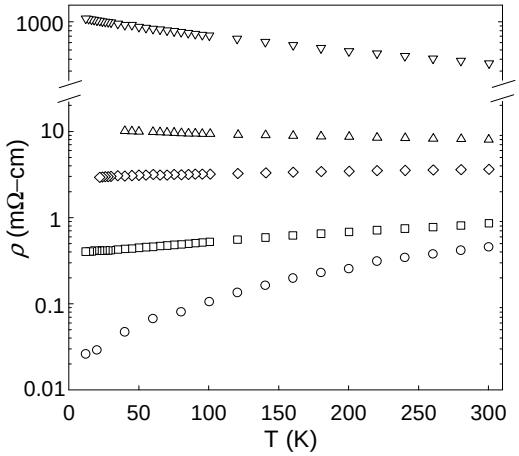

Figure 1.5: Resistivity (log scale) as a function of temperature for Na_xSi_{136} with x = 2.9 (∇), 5.1 (Δ), 8.2 (◊), 14.7 (□), and 24 (○). Reprinted with permission from Ref. 26. Copyright [2012]. American Chemical Society.

Gryko [25] used this degas method to create an essentially empty Si_{136} clathrate. This clathrate was measured to be a wide band gap semiconductor, holding promise for optoelectronic applications[5].

The thermal properties of type I and II clathrates of group 14 are also of great interest. Their unique thermal properties [2] are directly related to their guest-host interactions. The guest atom is weakly bound to the cage like framework [1], giving the guest atom the ability to move, or "rattle" inside the cage. This "rattling" behavior creates strong phonon scattering , which results in a low thermal conductivity in clathrates [1,2,3]. It has also been found that the heavier the atom and the greater the size difference between the guest and its cage, the lower the thermal conductivity[23]. The magnitude and temperature dependence of the guest atoms atomic displacement parameters (ADPs) is shown in Figure 1.6 [27].

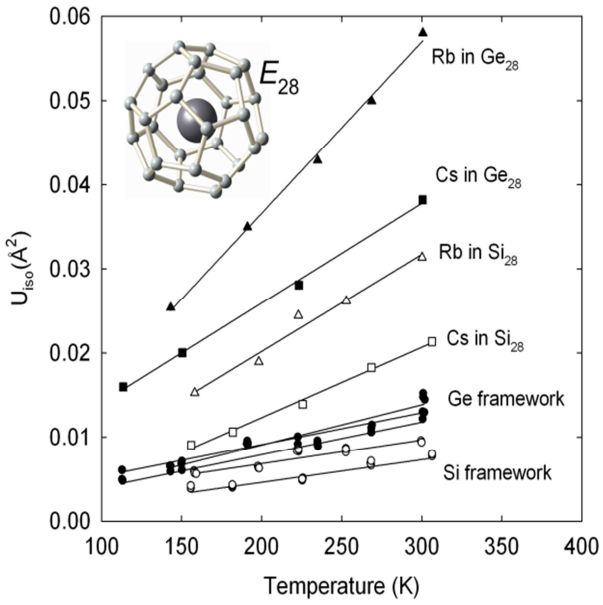

Figure 1.6: Temperature dependent isotropic atomic displacement parameters (U_{iso}) for the E_{28} guest as well as framework sites in $A_8Na_{16}E_{136}$ (A = Rb, Cs; E = Si, Ge)
Reprinted with permission from Ref. 27 Copyright [2002], American Institute of Physics.

This "rattling" behavior, that results in a lower thermal conductivity in various clathrates, has been one of the most interesting and important discoveries in thermoelectric research as it introduces the "phonon glass electron crystal" (PGEC) concept introduced by Slack et al.[28] . $Sr_8Ga_{16}Ge_{30}$, for example, exhibits a lattice thermal conductivity temperature dependence comparable to amorphous solids (Fig 1.7b). The PGEC concept refers to this quality that various clathrates have in exhibiting a thermal conductivity similar to amorphous materials, such as glass, while also exhibiting the electrical properties of crystalline materials. This is of great importance for thermoelectric research, as materials with low thermal conductivity and tunable electric properties may result in superior thermoelectric materials [2]. The "rattling" effect is clearly demonstrated in Fig 1.7a as the clathrates with heavier guest atoms and a greater size difference between the guest and cage have a lower lattice thermal conductivity.

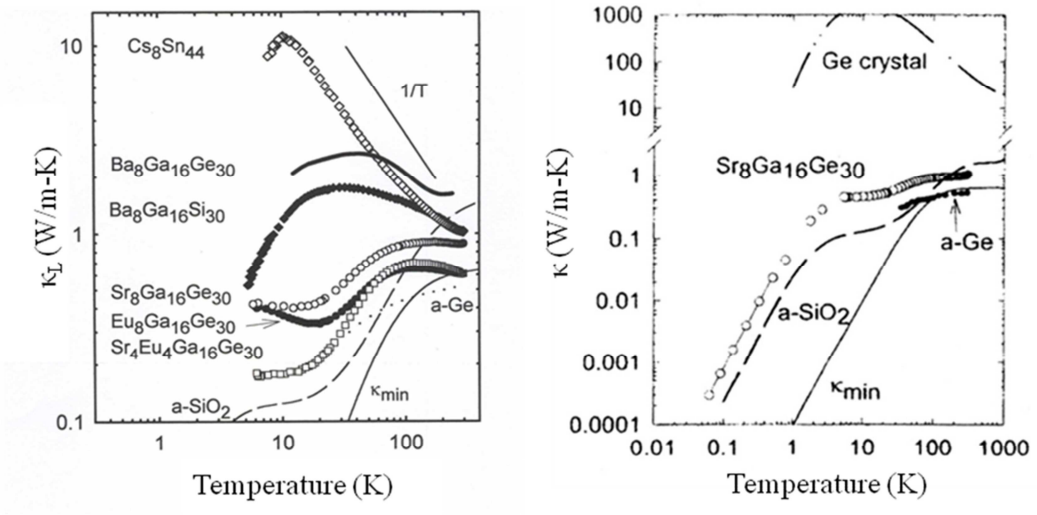

Figure 1.7: a) κ_L for several representative type I clathrates b) "Glass-like" κ for $Sr_8Ga_{16}Ge_{30}$

1.3. Applications

The interesting physical properties displayed by type I and II clathrates of group 14 show that these compounds hold promise for a variety of applications. One such application is thermoelectrics. The determination of the quality or "goodness" of a thermoelectric material is the dimensionless figure of merit, ZT [1]. ZT is calculated by the equation $ZT=S^2\sigma/\kappa$ with S being the Seeback coefficient, σ being the electric conductivity, and κ being the thermal conductivity with $\kappa= \kappa_L+ \kappa_e$, where κ_L is the lattice component of thermal conductivity and κ_e is the electrical component of thermal conductivity. Therefore in order to achieve a high ZT, a material must have a high "power factor", $S^2\sigma$, and low κ. However materials with high S generally have low σ , such as semiconductors, and materials with high σ generally have low S, such as metals (Figure 1.8)[29].

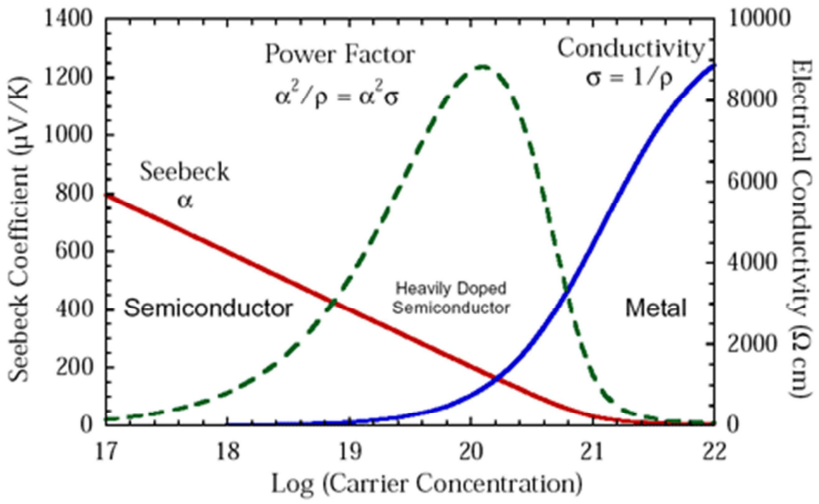

Figure 1.8: Variance of the seeback coefficient and electrical conductivity for semiconductors and metals. Reprinted with the permission of Reference 29. Copyright [2008]. Nature Publishing Group.

Therefore clathrates are great candidates for thermoelectric materials as they are able to exhibit low κ while also being able to change their dopant level as semiconductors[2].

Another area of great interest in clathrate research is that of optoelectronics. The semiconductor Si has been the standard bearer as the most important material in electronic devices [30]. Recently, amorphous Si has been revealed to have interesting optical properties in comparison to crystalline silicon (α-Si) [31]. However the low efficiency of a photoelectric device using crystalline or amorphous Si is a problem for mainstream optoelectronic applications[32]. An important discovery in clathrate research predicted a wide-band gap Si clathrate [33] and was later experimentally verified by Gryko et al. [5]. The empty type II Si_{136} clathrate synthesized by Gryko exhibits an expanded band gap of 2.0 eV (E_{gap} of α Si ~1.2 eV), qualifying it as a novel wide-band gap semiconductor with potential for photovoltaic applications (Figure 1.9).

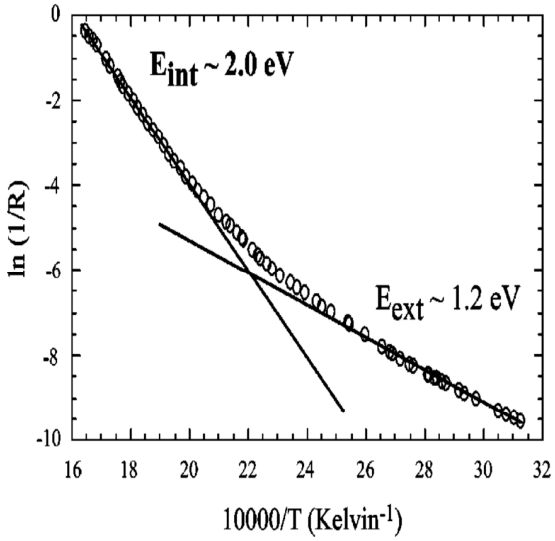

Figure 1.9: Si_{136} as a wide band gap material

Reprinted with the permission of Reference 5. Copyright [2008]. American Physical Society

Another important result that increases the potential of type II clathrates of group 14 for optoelectronic applications was the theoretical prediction by Moriguchi et al. [4] of possible band gap engineering by varying the clathrate composition. Moriguchi et al.[4] , using density functional techniques, having explored how the band gap of the clathrate-II silicon-germanium alloy, $Si_{136-x}Ge_x$, changes depending on composition. The authors found that by this band gap tuning it is not only possible to vary the band gap, but also to tune the $Si_{136-x}Ge_x$ clathrate to have a direct band gap. The results from the study indicated that the band gap could be continuously "tuned" in the visible range of the electromagnetic spectrum from values of 1.2 to 2 eV. Therefore the possibility of a type II clathrate being a wide-band gap Si semiconductor that has a direct band gap holds enormous potential in the field of photovoltaics and optoelectronics.

2. Pressure-mediated selective synthesis of type I and II Si-clathrates using Spark Plasma Sintering

2.1. Spark Plasma Sintering as a novel synthesis method

The search for new synthesis techniques is of great importance to experimental physicists and is one of the main components of this lab, the Novel Materials Laboratory at the University of South Florida. Recently, in collaboration with Dr. Yuri Grin's laboratory at the Max Planck Inst., this laboratory has optimized the use of spark plasma sintering (SPS) as a novel synthesis technique in the creation of single crystal and microcrystalline clathrates. SPS is a state of the art densification and consolidation technique, with numerous advantages over hot pressing[34] as a densification method due to the more uniform and local heating and the faster heating rates that the SPS employs [35,36,37]. In the process of consolidating a specimen, a DC current is sourced through the anode, through the die and specimen and then up through the cathode (Fig 2.1). This is done under vacuum and while the punch and die assembly is under uniaxial pressure (applied by the anode and cathode). The DC current allows SPS to achieve faster densification due to its faster heating rates [35,36,37]. More recently SPS has been used as a method to synthesis new materials [38,39,40]. Beekman et al. [41] also used SPS to synthesize single crystal $Na_{24}Si_{136}$ clathrates, being the first one to synthesize $Na_{24}Si_{136}$ in single crystal form.

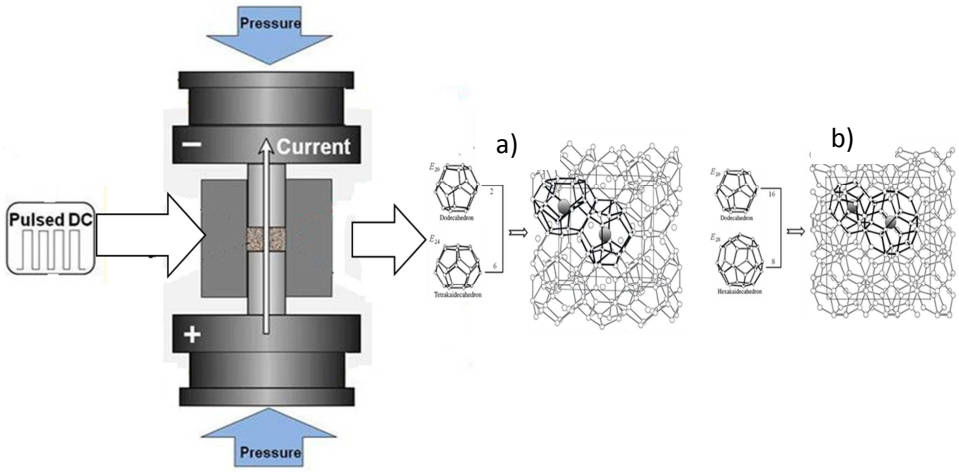

Fig 2.1: Spark Plasma Sintering setup illustrating the DC current flowing through the anode, through the die, and through the cathode -crystal structure of a) Na_8Si_{46} and b) $Na_{24}Si_{136}$
Reprinted with permission from Ref 41 and Ref 1. Copyright [2009], American Chemical Society.

Copyright [2001], Elsevier Books.

The DC current that is sourced through the specimen from the anode to the cathode allows mass transport of the ions to occur. Therefore, while the specimen is under uniaxial pressure, clathrate growth and crystal formation can occur. In this study, using SPS as a novel synthesis method, and by varying the temperature and uniaxial pressure of the SPS, one is able to selectively synthesize microcrystalline and single crystal type I Na_8Si_{46} and type II $Na_{24}Si_{136}$ clathrates.

2.2. Selective synthesis of crystalline and microcrystalline clathrates

The Na_4Si_4 precursor that was used for the reaction was synthesized by direct reaction of elemental Na (Alfa Aesar, 99.98%) and Si powder (Alfa Aesar, 99%). A Na:Si atomic ratio of 1.1:1 was placed in a tungsten crucible and sealed in a stainless steel canister in a nitrogen filled dry-box. The canister was then placed in a quartz tube, sealed under N_2, and reacted in a furnace at a temperature of 650° C for a reaction time of 36 hours. The resulting product was opened in the dry-box and resembled a dark grayish powder that was then coarsely ground.

The SPS investigations were carried out using the Thermal Technology, Inc. 10-3 system. Pulsed DC current, with pulse-on time of 36 ms and pulse-off time of 2 ms, was sourced through the anode, through the specimen and punch and die assembly, and finally through the cathode. The reaction took place at uniaxial pressures of 60, 80, and 100 MPa, at a reaction time of 30 minutes to 3 hours, and at reaction temperatures of 450°C, 550°C, 600°C and 650°C. All reactions in the SPS chamber took place under a vacuum of 10^{-3} Torr. The resulting product was allowed to cool to a temperature of 50°C and washed with distilled water and ethanol to remove any unreacted precursor.

Single-crystal XRD data of Na_8Si_{46} and $Na_{24}Si_{136}$ crystals were obtained at 293 K on a STOE diffractometer using a graphite monochromator and a Mo K_α fine-focus sealed tube with a wavelength of 0.71073 Å. The single crystal refinement was done at Northwestern University. Structural refinements were performed using SHELXL-97 (Tables 2.1 – 2.5) .

Table 2.1. Single-crystal XRD refinement data for Na_8Si_{46} and $Na_{24}Si_{136}$.

Composition	Na_8Si_{46}	$Na_{24}Si_{136}$
Formula weight	1476.06	4372.00
Crystallinity	single-crystal	single-crystal
Largest Crystal size (mm)	0.20	0.49
Crystal system, space group	Cubic, $Pm\bar{3}n$	Cubic, $Fd\bar{3}m$
Lattice parameter, *a*/Å	10.1961(7)	14.71560(10)
Calculated density / gcm^{-3}	2.312	2.280
2θ (deg.)	4.90 to 38.07	4.59 to 38.04
R	0.0520	0.0662
wR	0.0358	0.0885
Goodnes of fit on χ^2	1.003	1.577

Table 2.2. Refined atomic positions, occupancies, and isotropic atomic displacement parameters (U_{iso}) for single-crystal Na_8Si_{46}.

Atom	***x/a***	***y/a***	***z/a***	**Occ.**	U_{iso} **(Å)**
Na1	0	0	0	1	0.0185(4)
Na2	0	0.5	0.25	1	0.0416(8)
Si1	0.11733(3)	0.30777(4)	0	1	0.00681(7)
Si2	0.18413(2)	0.18413(2)	0.18413(2)	1	0.00677(7)
Si3	0.25	0.5	0	1	0.00666(14)

Table 2.3. Refined anisotropic atomic displacement parameters (U_{ij}/Å) for single-crystal Na_8Si_{46}.

Atom	U_{11}	U_{22}	U_{33}	U_{12}	U_{13}	U_{23}
Na1	0.0185(4)	0.0185(4)	0.0185(4)	0	0	0
Na2	0.0490(10)	0.0490(10)	0.0267(10)	0	0	0
Si1	0.00653(14)	0.00661(15)	0.00729(15)	-0.00057(13)	0	0
Si2	0.00677(7)	0.00677(7)	0.00677(7)	-0.00024(8)	-0.00024(8)	-0.00024(8)
Si3	0.0070(3)	0.00651(19)	0.00651(19)	0	0	0

Table 2.4. Refined atomic positions, occupancies, and isotropic atomic displacement parameters (U_{iso}) for single-crystal $Na_{24}Si_{136}$.

Atom	***x/a***	***y/a***	***z/a***	**Occ.**	U_{iso} **(Å)**
Na1	0	0	0	1	0.0195(8)
Na2	0.3750	-0.1250	-0.1250	1	0.118(6)
Si1	0.1250	0.1250	0.1250	1	0.0066(5)
Si2	0.18265(4)	0.06735(4)	-0.12117(6)	1	0.00652(16)
Si3	0.21800(6)	0.03200(6)	0.03200(6)	1	0.0064(2)

Table 2.5. Refined anisotropic atomic displacement parameters (U_{ij}/Å) for single-crystal $Na_{24}Si_{136}$.

Atom	U_{11}	U_{22}	U_{33}	U_{12}	U_{13}	U_{23}
Na1	0.0195(8)	0.0195(8)	0.0195(8)	-0.0020(8)	-0.0020(8)	-0.0020(8)
Na2	0.118(6)	0.118(6)	0.118(6)	0	0	0
Si1	0.0066(5)	0.0066(5)	0.0066(5)	0	0	0
Si2	0.0065(2)	0.0065(2)	0.0066(3)	-0.0009(2)	0.00016(18)	-0.00016(18)
Si3	0.0064(2)	0.0064(2)	0.0064(2)	0.0000(3)	0.0000(3)	0.0000(3)

Powder X-ray diffraction (XRD) patterns were collected with a Bruker D8 Focus diffractometer in Bragg-Brentano geometry using Cu $K_{\alpha,\beta}$ radiation and a graphite monochromator. NIST Si 640c internal standard was used for determination of lattice parameters. Scanning electron micrographs (SEM) were collected using a JEOL JSM-6390LV, and energy dispersive X-ray spectroscopic (EDS) data were collected using an Oxford INCA X-Sight 7582M. The results of the powder refinement are displayed in

Tables 2.6-2.8 and in Figures 2.2 and 2.3. All crystallographic results of single crystal and powder refinement are consistent with those obtained previously [24,42].

Table 2.6. Crystallographic data from the Rietveld refinements of microcrystalline specimens of the clathrate-I and II phases.

Refined Composition	Na_8Si_{46}	$Na_{24}Si_{136}$
Formula weight	1464.442	4344.376
Crystallinity	microcrystalline	microcrystalline
Crystal system, space group	Cubic, $Pm\bar{3}n$	Cubic, $Fd\bar{3}m$
Lattice parameter, *a*/Å	10.1998(1)	14.7167(1)
Calculated density / gcm^{-3}	2.292	2.279
2θ (deg.)	10 to 120	10 to 120
cRp	0.0809	0.0769
cRwp	0.1056	0.1063
Goodnes of fit on χ^2	1.316	1.891
Rp	0.1035	0.0897
Rwp	0.1266	0.1161

Table 2.7. Refined atomic positions, occupancies, and isotropic atomic displacement parameters (U_{iso}) for microcrystalline Na_8Si_{46}.

Atom	***x/a***	***y/a***	***z/a***	**Occ.**	**U_{iso} (Å)**
Na1	0	0	0	1	0.010
Na2	0.5	0	0.25	1	0.0714
Si1	0.30817	0.12030	0	1	0.0175
Si2	0.18049	0.18049	0.18049	1	0.01223
Si3	0.5	0.25	0	1	0.0179

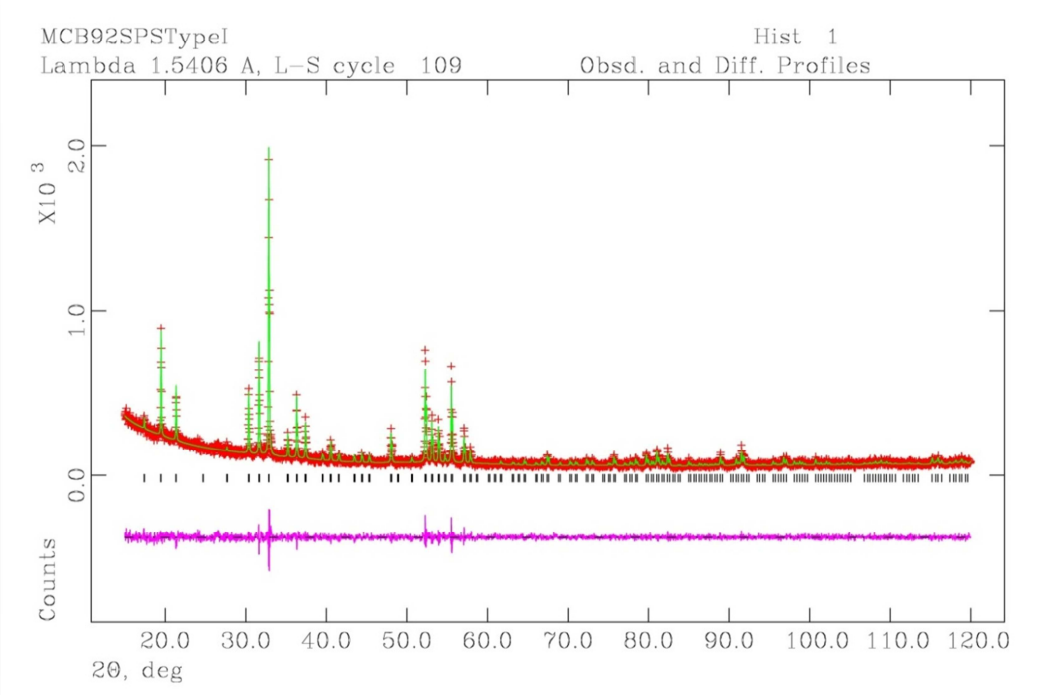

Figure 2.2 Observed (red crosses), calculated (green curve), and difference (purple curve) powder X-ray diffraction patterns for microcrystalline Na_8Si_{46}. Black tick marks indicate reflection positions for the Na_8Si_{46} phase.

Reprinted with the permission of Reference 64. Copyright [2013]. American Chemical Society.

Table 2.8. Refined atomic positions, occupancies, and isotropic atomic displacement parameters (U_{iso}) for microcrystalline $Na_{24}Si_{136}$.

Atom	***x/a***	***y/a***	***z/a***	**Occ.**	U_{iso} **(Å)**
Na1	0	0	0	1	0.0250
Na2	0.375	0.375	0.375	1	0.1677
Si1	0.125	0.125	0.125	1	0.0168
Si2	0.21809	0.21809	0.21809	1	0.0065
Si3	0.06652	0.06652	0.37226	1	0.0146

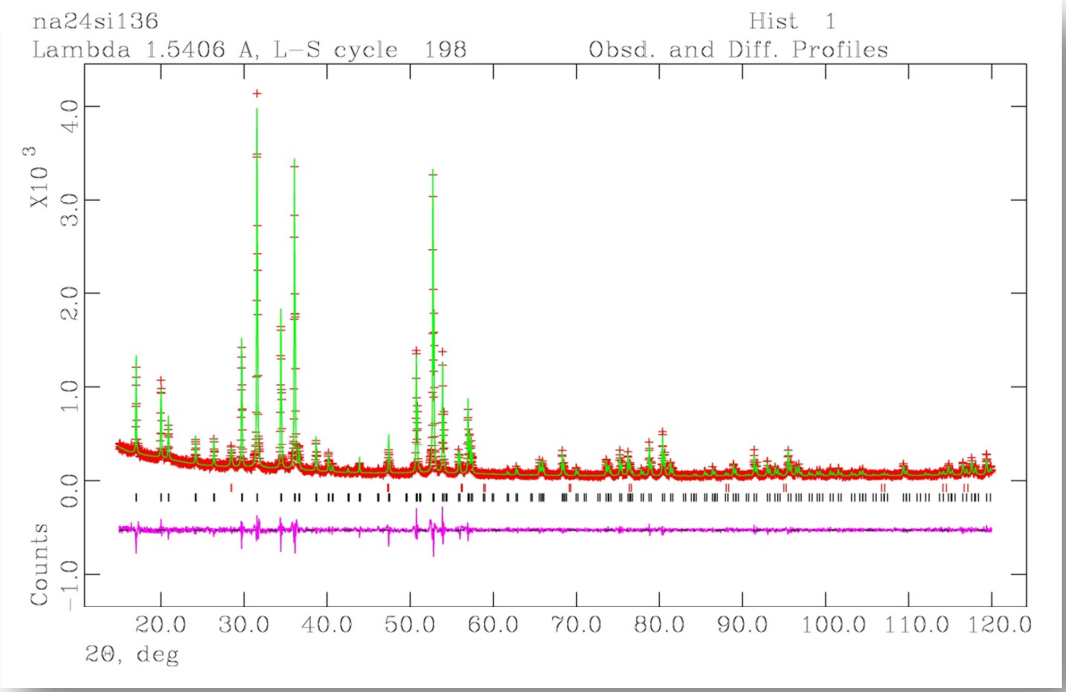

Figure 2.3 Observed (red crosses), calculated (green curve), and difference (purple curve) powder X-ray diffraction patterns for microcrystalline $Na_{24}Si_{136}$. Black tick marks (lower) indicate reflection positions for the $Na_{24}Si_{136}$ phase; red tick marks (upper) indicate reflection positions for the Si impurity phase. Reprinted with the permission of Reference 64. Copyright [2013]. American Chemical Society.

2.3 Temperature and pressure effects

Maintaining a uniaxial pressure of 100 MPa and reacting for a reaction time of 3 hours under a dynamic vacuum, phase pure single crystal specimens were obtained at temperatures of 450°C and 600°C, respectively. At 450 °C and a uniaxial pressure of 100 MPa, single crystals of the type I clathrate, Na_8Si_{46}, formed. At 600 °C, single crystals of the type II clathrate, $Na_{24}Si_{136}$, formed. At temperatures below 450 °C no clathrate formation was observed and at a temperature of 650 °C only α-Si was obtained. The

selective synthesis of single-crystal clathrates at 100 MPa is displayed below in Figure 2.4.

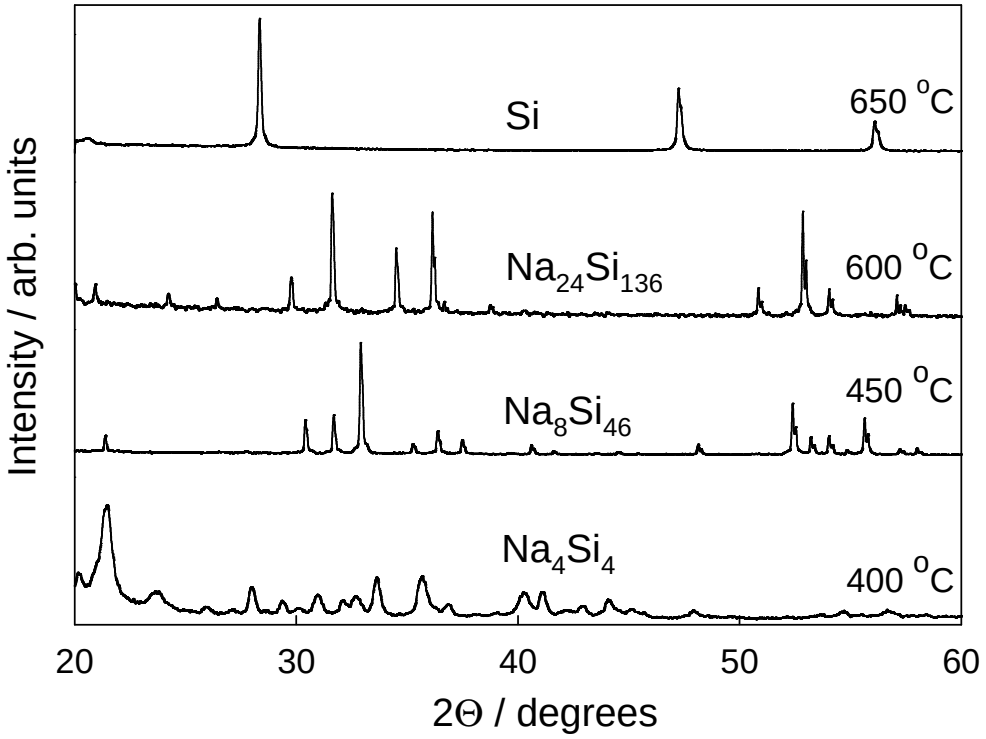

Figure 2.4- X-ray diffraction patterns of powdered Na_8Si_{46} and $Na_{24}Si_{136}$, collected from crushed single crystals, Na_4Si_4 and Si demonstrating the selective synthesis of single-crystal clathrates at 100 MPa. Reprinted with the permission of Reference 64. Copyright [2013]. American Chemical Society.

This is the first time that single crystals of the type I clathrate, Na_8Si_{46}, have been synthesized by the SPS method. The synthesis of single-crystals of clathrates is of great importance as only single crystals are free of any minor clathrate or α-Si impurities, which is typically seen in Na_8Si_{46} and Na_xSi_{136} clathrates in microcrystalline form [10,11,43,44]. Single-crystals are also preferred for physical property measurements as consolidation and densification is not needed [45].

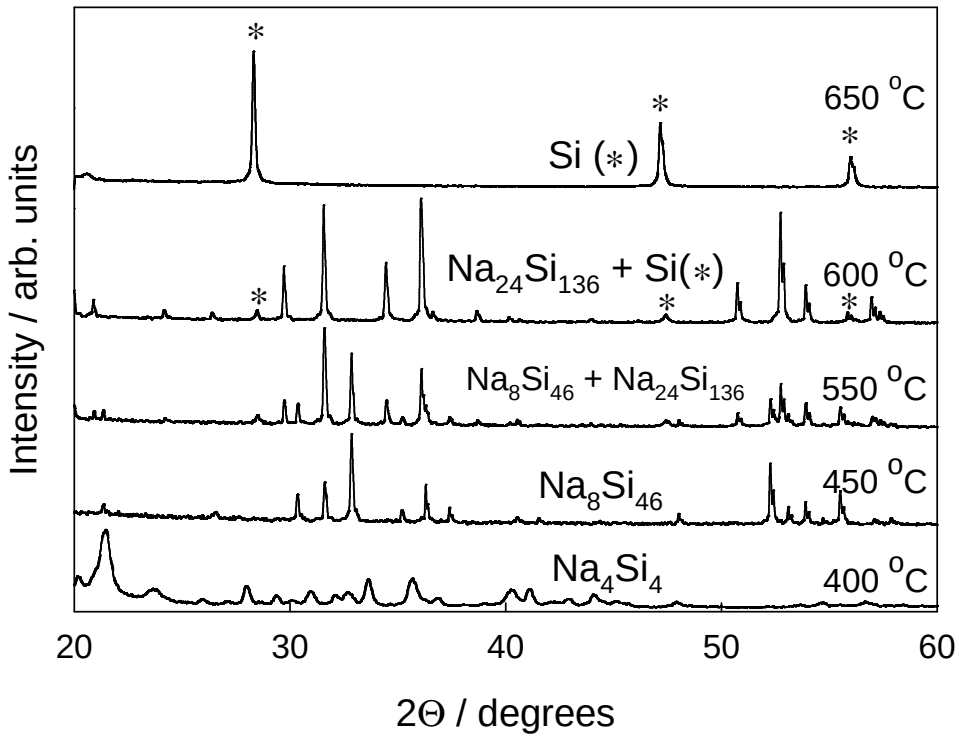

Figure 2.5- X-ray (Cu $K_{\alpha,\beta}$) diffraction patterns of microcrystalline Na_4Si_4, Na_8Si_{46}, $Na_{24}Si_{136}$ and Si demonstrating the selective synthesis of microcrystalline clathrate specimens at 60 MPa. Reprinted with the permission of Reference 64. Copyright [2013]. American Chemical Society.

At a uniaxial pressure of 60 MPa, under a dynamic vacuum and at a reaction time of 3 hours, selective synthesis of microcrystalline clathrates was also obtained (Figure 2.5). At a temperature of 450 °C and a uniaxial pressure of 60 MPa, the type I clathrate, Na_8Si_{46}, formed. At 600 °C, the type II clathrate, $Na_{24}Si_{136}$, with an impurity of 5 wt % α-Si, formed. The presence of α-Si in microcrystalline Na_xSi_{136} clathrates is typically observed [10,11,43,44]. At temperatures below 450 °C no clathrate formation was observed and at a temperature of 650 °C only α-Si was obtained. At a temperature of 550° C the resulting product was a mixture of type I and II NaSi microcrystalline clathrates. The selective synthesis of microcrystalline clathrates at 60 MPa is shown in Figure 2.5.

As shown from Figures 2.4 and 2.5 the variance of the uniaxial pressure during the synthesis process changes the size of the crystallinity product. Table 2.9 displays the processing conditions for the SPS synthesis of clathrates and shows how the crystallinity of the clathrates change as the pressure is increased. The grain size of the powders was calculated using the Debye-Scherrer equation [46,47]. The size of the single crystals was obtained from SEM analyses.

Table 2.9 Processing conditions for SPS synthesis from the precursor Na_4Si_4.

***P* (MPa)**	**Phase**	***T* (^{0}C)**	**Crystallinity**	***L* (μm)**
60	clathrate-I	450	microcrystalline	10
80	clathrate-I	450	microcrystalline	10
100	clathrate-I	450	single crystal	150
60	clathrate-I+II	550	microcrystalline	10
80	clathrate-I+II	550	microcrystalline & single crystal	10/150
100	clathrate-I+II	550	microcrystalline & single crystal	10/150
60	clathrate-II	600	microcrystalline	15
80	clathrate-II	600	single crystal	50
100	clathrate-II	600	single crystal	250
100	Silicon	650	nano-crystalline	0.065

For the $Na_{24}Si_{136}$ clathrate, as the uniaxial pressure is increased from 60 MPa to 80 MPa, small single crystals of 50 microns in size appear. As the uniaxial pressure is increased to 100 MPa, one obtains the largest crystal size of 250 microns for $Na_{24}Si_{136}$. Therefore for the $Na_{24}Si_{136}$ clathrate it appears that the increase in uniaxial pressure causes the crystal formation to occur and that the crystal size is increasing with increasing uniaxial pressure. For the Na_8Si_{46} clathrate, as the uniaxial pressure is increased from 60 MPa to 80 MPa, the clathrate is still in microcrystalline form. As the uniaxial pressure

is increased to 100 MPa one obtains single-crystals of Na_8Si_{46}, with the largest crystal size being 150 microns. Therefore it appears that for the type I Na_8Si_{46} clathrate there is a threshold pressure of 100 MPa for single-crystal formation.

Another interesting result in this study came after measuring the grain size of the α-Si that was obtained at a pressure of 60 MPa, reaction time of 3 hours, and a reaction temperature of 650 °C. Using the Debye-Scherrer method to measure the grain size of the α-Si product indicated that the α-Si was in nano-crystalline form with a grain size of 65 nm. This is an important result as Si nanoparticles are of great interest to green chemistry [48,49]. Therefore, this could indicate that SPS can be used as a novel synthesis method of Si nanoparticles.

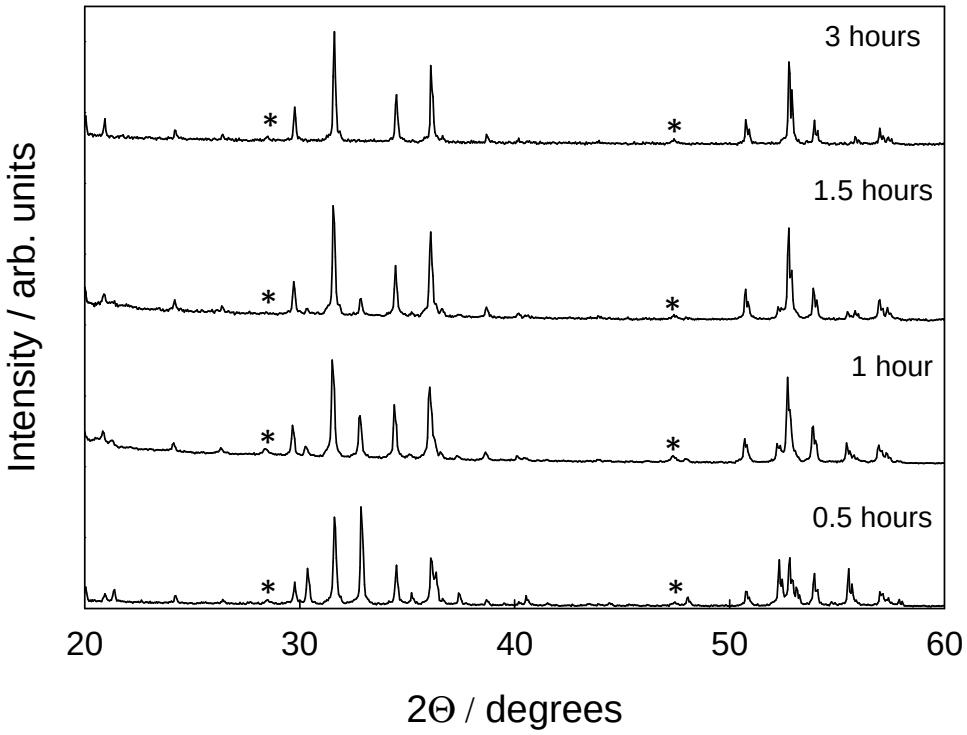

Figure 2.6- X-ray powder patterns showing the type-I and II clathrate fractions as a function of reaction time at 600°C. α-Si is indicated by (∗).

The variance of the product by changing the reaction time for a reaction temperature of 600°C and uniaxial pressure of 60 MPa was also studied (Figure 2.6). All previous results were for a reaction time of 3 hours. At a reaction time of 30 min and at a reaction temperature of 600°C, the result was a product of 60 wt % type I clathrate and 40 wt % type II clathrate. At a reaction time of 1 hr and at a reaction temperature of 600°C, the result was a product of 70 wt % type II clathrate and 30 wt % type I clathrate. As the reaction time increased to 1 hr and 30 min and at a reaction temperature of 600°C, the result was a product of 90 wt % type II clathrate and 10 wt % type I clathrate. At a reaction time of 3 hours, the type II clathrate phase without any type I impurities was observed. These results are another step in understanding the fundamental physics of the clathrate formation process that occurs during SPS synthesis.

By varying the uniaxial pressure and the reaction temperature during SPS processing, one is able to selectively synthesize microcrystalline and single-crystal type I and type II clathrates. The variance of clathrate purity by changing the time of the reaction was also studied. Finally, this study also indicated that the SPS has the potential to be a new synthesis method for growing Si nanoparticles.

3. Synthesis of Na_8Si_{46} and $Na_{24}Si_{136}$ by oxidation of Na_4Si_4 by decomposition of an ionic liquid

3.1. Overview of ionic liquid synthesis

The use of ionic liquids as a new low-temperature synthesis method of inorganic materials has recently created enormous interest. Ionic liquids (IL) are organic salts that consist entirely of ions[50]. Ionic Liquids were first discovered and analyzed by Prof Atwood et al. in the 1970's who discovered that most ILs have organic cations and inorganic anions [51]. The recent interest in ILs is due to their ability of being used as a solvent of inorganic compounds, and in doing so having an assortment of chemical reactions at one's disposal as a result [50]. Ionic liquids are also considered as molten-salt solvents as they are non-aqueous and thermodynamically stable at room temperature [52]. Ionic liquids display an array of favorable properties that allow them to be of great interest as a low-temperature synthesis method and as a green solvent[50]. Some of these beneficial properties of ILs are their low melting points (below 100°C), their wide range of thermal stability (stable below 330°C), their low to negligible vapor pressures, and the ability to adjust their electrical properties based on composition [52,53].

Recently, Guloy et al. used these favorable properties to use ILs as a solvent to create a guest-free type II Ge_{136} clathrate [54]. This was accomplished by oxidizing the precursor $Na_{12}Ge_{17}$ in the ionic liquid n-dodecyltrimethylammonium chloride and $AlCl_3$ ($DTAC/AlCl_3$)[54]. Guloy et al. also used this method to synthesize the type II clathrate $K_{8.6}Ge_{136}$ through oxidation of the precursor K_4Ge_4 in the IL ($DTAC/AlCl_3$) and by

further annealing of the resulting product[21]. Further analysis of these chemical reactions indicates that as the ILs thermally decompose; they release a variety of compounds. These compounds that are released are HCl, $N(CH_3)_3$, and NH_4Cl; with the gaseous HCl seen to be as the main oxidizing agent[55]. A group from the Max Planck Inst. in Dresden, Germany, simplified this procedure by obtaining the gaseous HCl from the thermal decomposition of NH_4Cl[56]. Bohme et al. through this procedure used the oxidation agent, HCl, to create a redox reaction that resulted in $(Na, K)_{8-x}Si_{46}$ type I clathrates[56] and the $Na_2Ba_6Si_{46}$ type I clathrate [57] while Liang et al. also used this procedure to create a type I $Ba_{8-x}Si_{46}$ clathrate [58]. Liang's use of this low-temperature synthesis method is significant as previously the synthesis of type I clathrate Ba_8Si_{46} was only possible under high temperature and high pressure conditions[59]. In this study, through the thermal decomposition of the IL ($DTAC/AlCl_3$), we were able to selectively synthesize the fully occupied type I Na_8Si_{46} and type II $Na_{24}Si_{136}$ clathrates.

3.2. Synthesis of type I Na_8Si_{46} and type II $Na_{24}Si_{136}$

The precursor used in the synthesis of the type I and II NaSi clathrates is Na_4Si_4. The synthesis of the precursor Na_4Si_4 is thoroughly described in section 2. The IL used was a mixture of n-dodecyltrimethylammonium chloride (Sigma Aldrich, 99 %) and $AlCl_3$ (Alfa Aesar, 99.99 % ultra-dry). The IL was placed at the bottom of a quartz tube and was not mixed or stirred. The precursor Na_4Si_4 was placed in a separate smaller open glass vial and placed on top of the IL mixture in the quartz tube. The spatial separation of the precursor and IL is done in order to ensure no formation of unwanted amorphous phases (as is seen from Guloy et al. when they mixed the precursor and IL in the process of creating Ge_{136} and $K_{8.6}Ge_{136}$). All preparations were done in a dry, nitrogen filled

glove box. The quartz tube containing the IL and spatially separated precursor was then sealed under vacuum. The sealing was done while the bottom of the quartz tube (containing the IL) was placed in an ice bath in order to prevent premature decomposition of the IL. The sealed length of the quartz tube varied from 4.5 – 8 inches.

The sealed quartz tube containing the IL and spatially separated Na_4Si_4 precursor was then placed in a furnace and heated at a rate of 1°C/min to final temperatures of 120°C to 310°C (Fig 3.1). Above 310°C the IL turned black indicating total decomposition of the IL. The quartz tube was reacted in the furnace for reaction times of 1 hour to 48 hrs. The quartz tube was then rapidly air quenched and placed in a sand bath. Once cool, the vial containing the initial Na_4Si_4 precursor was removed from the quartz tube in a nitrogen filled glove bag. Part of the resulting product was placed on an air-sensitive XRD slide while the remaining product was washed with ethanol and distilled water. Analysis of the pre-washed product indicated the formation of NaCl and unreacted Na_4Si_4 precursor. The washed product was dried in air and analyzed on a XRD slide. Powder refinement was done with the aid of the GSAS[60] and EXPGUI[61] software.

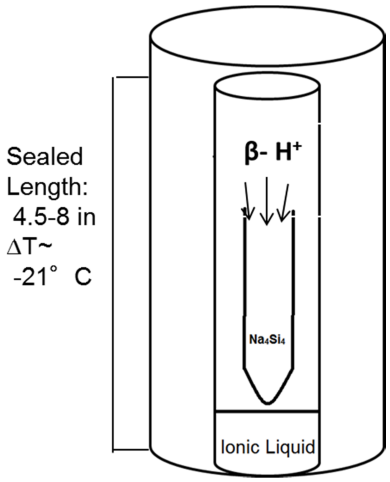

Figure 3.1: Experimental setup of the IL synthesis method

3.3. Results and Crystallographic Data

Through oxidation of the precursor, Na_4Si_4, fully occupied type I Na_8Si_{46} and type II $Na_{24}Si_{136}$ clathrates were synthesized. This redox reaction was caused through the thermal decomposition of the IL DTAC/$AlCl_3$. As the IL thermally decomposes it releases acidic protons β-H+ supplied by the DTAC and chloride ions supplied by the $AlCl_3$ which combine to form HCl vapor (among other compounds) that drives the redox reaction[55]. As the reaction continues the HCl is further reduced to H_2 as the chloride reacts with the akali metal anions, forming a stable byproduct, such as NaCl as observed in this study. The observation of NaCl in the prewashed product and the fact that the reaction temperatures were significantly lower than the decomposition temperatures of Na_4Si_4 in vacuum (~375°C) [11] while also being lower than the decomposition temperatures of Na_8Si_{46} and Na_xSi_{136} [43,24,13,62,12,17,42] verify that the clathrates were formed as a result of the redox reaction.

$Na_{24}Si_{136}$ clathrates readily formed at reaction temperatures of 210°C to 240°C at reaction times of 24 hours. The highest yield (20% by weight) of $Na_{24}Si_{136}$ with only a 5% by weight impurity of α-Si was synthesized at a reaction temperature of 210° C for a reaction time of 24 hours (Fig 3.2). Phase pure and high yield (20% by weight) Na_8Si_{46} was synthesized at a reaction temperature of 240°C at a reaction time of 8 hours (Fig 3.3). Reaction times longer than 48 hours resulted in α-Si and amorphous phases.

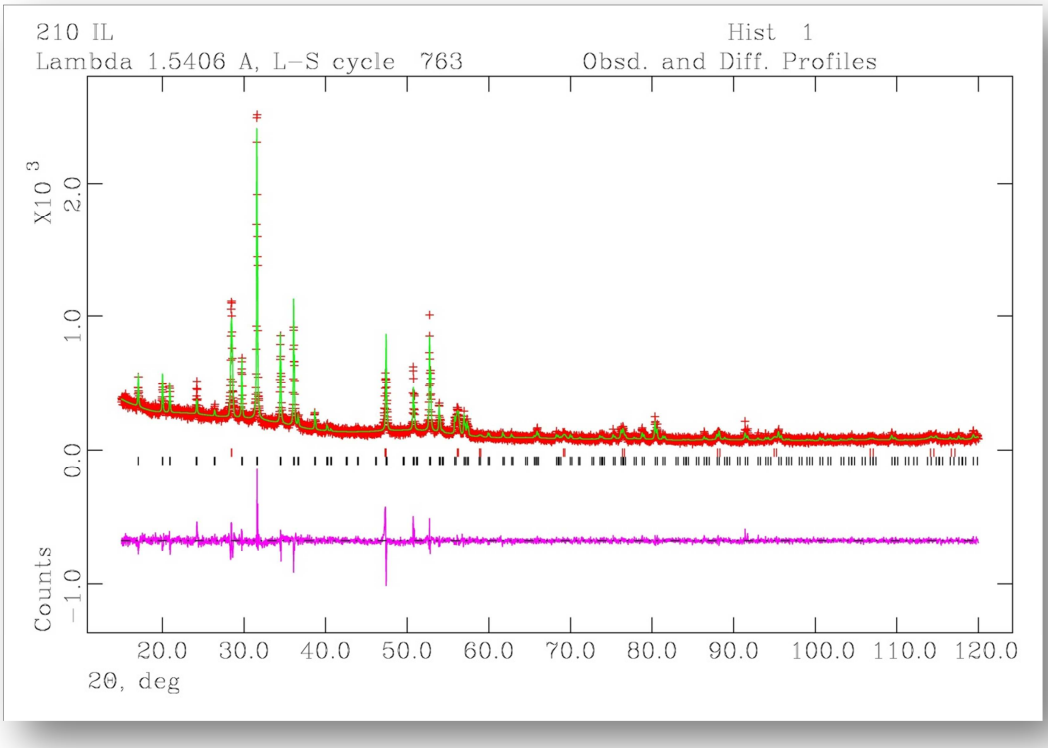

Figure 3.2: Observed (red crosses), calculated (green curve), and difference (purple curve) powder X-ray diffraction patterns for microcrystalline $Na_{24}Si_{136}$. Black tick marks (lower) indicate reflection positions for the $Na_{24}Si_{136}$ phase; red tick marks (upper) indicate reflection positions for the Si impurity phase.

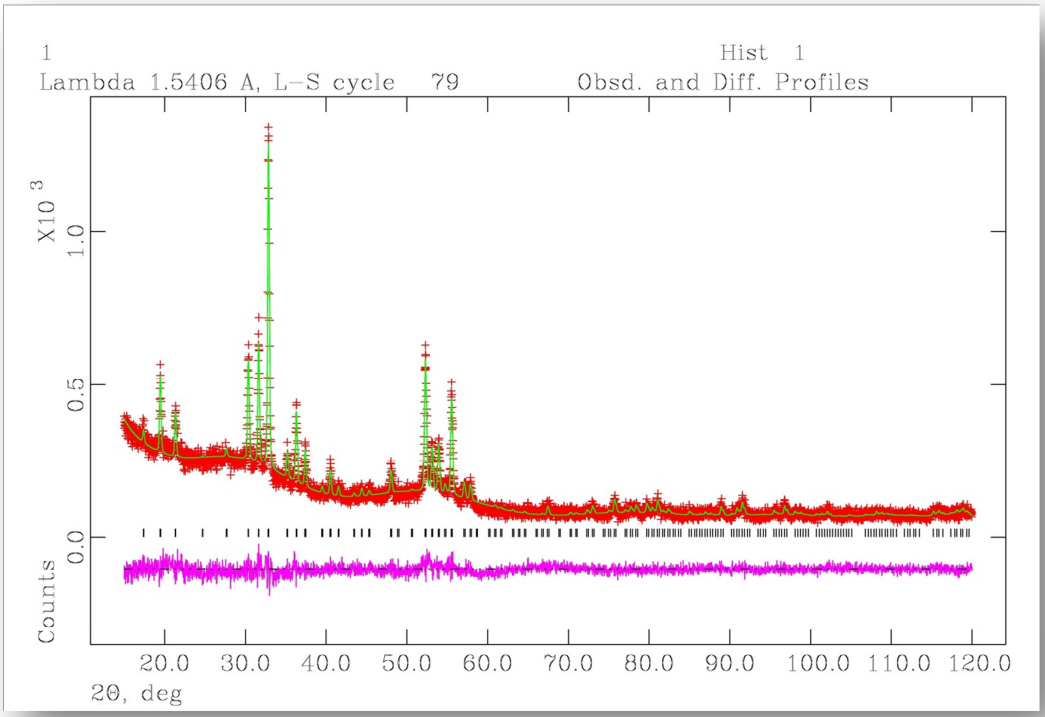

Figure 3.3 Observed (red crosses), calculated (green curve), and difference (purple curve) powder X-ray diffraction patterns for microcrystalline Na_8Si_{46}. Black tick marks indicate reflection positions for the Na_8Si_{46} phase.

One is able to use this method to selectively synthesize the NaSi clathrates by varying and optimizing the reaction time and temperature. Since the vapor pressures of ionic liquids are very low, one is able to have some sort of control of the vapor pressures by varying the reaction temperatures; thereby controlling the oxidation rate of the reaction. The oxidation rate of the reaction is important as the temperature needs to be substantially high enough to allow structural rearrangements of the ions to occur, but also low enough in order that the Na is not completely removed from the precursor. The reaction time needs to be optimized as if the redox reaction is allowed to continue on indefinitely, the precursor will be completely oxidized with the result of α-Si and

amorphous phases. Therefore, optimizing the reaction time and temperature, achieves this oxidation rate balance and allows clathrate formation. The resulting microcrystalline clathrate products were analyzed via an XRD and refined through the GSAS and EXPGUI software. The results of the refinement indicated full occupancy of the Na and Si crystallographic sites for both the type I Na_8Si_{46} and type II $Na_{24}Si_{136}$ clathrates. The results of the refinement are summarized in Tables 3.1- 3.4 below.

Table 3.1. Refined atomic positions, occupancies, and isotropic atomic displacement parameters (U_{iso}) for microcrystalline Na_8Si_{46}.

Atom	***x/a***	***y/a***	***z/a***	**Occ.**	U_{iso} **(Å)**
Na1	0	0	0	1	0.0627
Na2	0.5	0	0.25	1	0.0546
Si1	0.30981	0.11762	0	1	0.0162
Si2	0.18483	0.18483	0.18483	1	0.0181
Si3	0.5	0.25	0	1	0.0241

Table 3.2 Refined anisotropic atomic displacement parameters (U_{ij}/Å) for microcrystalline Na_8Si_{46}.

Atom	U_{11}	U_{22}	U_{33}	U_{12}	U_{13}	U_{23}
Na1	0.06271	0.06271	0.06271	0	0	0
Na2	0.05463	0.05463	0.05463	0	0	0
Si1	0.01620	0.01620	0.01620	0	0	0
Si2	0.01812	0.01812	0.01812	0	0	0
Si3	0.02409	0.02409	0.02409	0	0	0

Table 3.3 Refined atomic positions, occupancies, and isotropic atomic displacement parameters (U_{iso}) for microcrystalline $Na_{24}Si_{136}$.

Atom	***x/a***	***y/a***	***z/a***	**Occ.**	U_{iso} **(Å)**
Na1	0	0	0	1	0.0300
Na2	0.375	0.375	0.375	1	0.1000
Si1	0.125	0.125	0.125	1	0.0050
Si2	0.21886	0.21886	0.21886	1	0.0097
Si3	0.06686	0.06686	0.37948	1	0.0054

Table 3.4 Refined anisotropic atomic displacement parameters (U_{ij}/Å) for microcrystalline $Na_{24}Si_{136}$.

Atom	U_{11}	U_{22}	U_{33}	U_{12}	U_{13}	U_{23}
Na1	0.03000	0.03000	0.03000	0	0	0
Na2	0.10000	0.10000	0.10000	0	0	0
Si1	0.00500	0.00500	0.00500	0	0	0
Si2	0.00970	0.00970	0.00970	0	0	0
Si3	0.00536	0.00536	0.00536	0	0	0

The use of ionic liquids as solvents or gaseous sources to create inorganic compounds such as clathrates is of great interest. This low-temperature synthesis method has been

used and can be used to create new inorganic compounds. In this study, by optimizing the reaction temperature and reaction time, and through the thermal decomposition of the IL DTAC/$AlCl_3$, one is able to selectively synthesize fully occupied type I Na_8Si_{46} and type II $Na_{24}Si_{136}$ clathrates. The clathrate formation employed through this synthesis method should be further investigated as a tool to synthesize novel materials [63] and to create a type II Si_xGe_y clathrate that is of interest for optoelectronic applications[4].

4. Synthesis of microcrystalline $Na_8Ge_3Si_{38}$ by SPS synthesis

The spark plasma sintering (SPS) technique has generally been used for state of the art densification and consolidation of powders due to the fast heating rates and more uniform heating, as compared with other consolidation techniques[36,37]. In spark plasma sintering, a pulsed DC current is sourced through a specimen enclosed in a punch and die assembly placed in-between two electrodes (Fig 2.1). A more detailed analysis of the SPS is covered in section 2. Recently, spark plasma sintering has been employed as a novel synthesis tool of inorganic clathrates [41,64]. Beekman et al.[41] used the SPS to synthesize single crystals of the type II $Na_{24}Si_{36}$ clathrate and Stefanoski et al. [64] used the SPS as a method to selectively synthesize microcrystalline and single crystal type I Na_8Si_{46} and type II $Na_{24}Si_{136}$ clathrates.

In this study, the type I clathrate $Na_8Ge_3Si_{38}$ has been synthesized via the spark plasma sintering (SPS) technique.

4.1. Synthesis

The Na_2SiGe precursor was synthesized by direct reaction of elemental Na (Alfa Aesar, 99.98%) and SiGe powder (provided from Dr. S. Bhattacharya of the Bhabha Atomic Research Center, Mumbai, India). The SiGe alloy (50:50 ratio) was crushed to 425 mesh. Na:SiGe with a molar ratio of 1.85:1 was placed inside a tungsten crucible that was inside a sealed stainless steel canister, and reacted at 650 ^oC for 48

hours. The resulting product was a dark gray crystalline material that was used as the precursor in SPS processing.

The SPS investigations were carried out using the Thermal Technology, Inc. 10-3 system. The Na_2SiGe precursor was loaded in a graphite die. Tantalum foil was used to prevent direct reaction between the precursor and the graphite die and punches. Pulsed DC current, with pulse-on time of 36 ms and pulse-off time of 2 ms, was sourced through the precursor and die from the bottom electrode (anode) to the top electrode (cathode) while under 100 MPa of uniaxial pressure (applied by the anode and cathode) in a vacuum of 10^{-3} Torr for 3 hours after flushing the chamber three times with high purity N_2. The product of the reaction was separated from any unreacted Na_2SiGe by washing with ethanol and distilled water. The type I clathrate $Na_8Ge_3Si_{38}$ was obtained at a chamber temperature of 450 ^oC and at a reaction time of 3 hours.

Powder XRD patterns were collected with a Bruker D8 Focus diffractometer in Bragg-Brentano geometry using Cu $K_{\alpha,\beta}$ radiation and a graphite monochromator. NIST Si 640c internal standard was used for determination of lattice parameters. SEM micrographs were collected using a JEOL JSM-6390LV and EDS data were collected using an Oxford INCA X-Sight 7582M.

4.2. Crystal structure

Phase pure microcrystalline $Na_8Ge_3Si_{38}$ type I clathrate was obtained at a chamber temperature of 450 ^oC under vacuum, a uniaxial pressure of 100 MPa and for a reaction time of 3 hours (Figure 4.2). Experiments at reaction temperatures under 450 ^oC did not result in clathrate formation and experiments at reaction temperatures above 450 ^oC resulted in the presence of a SiGe impurity. Experiments at the temperature of 550 ^oC

resulted in the complete removal of the Na from the precursor resulting in a 100% SiGe product. The redox reaction that enables the formation of the clathrate structure in the SPS is described thoroughly in section 2.

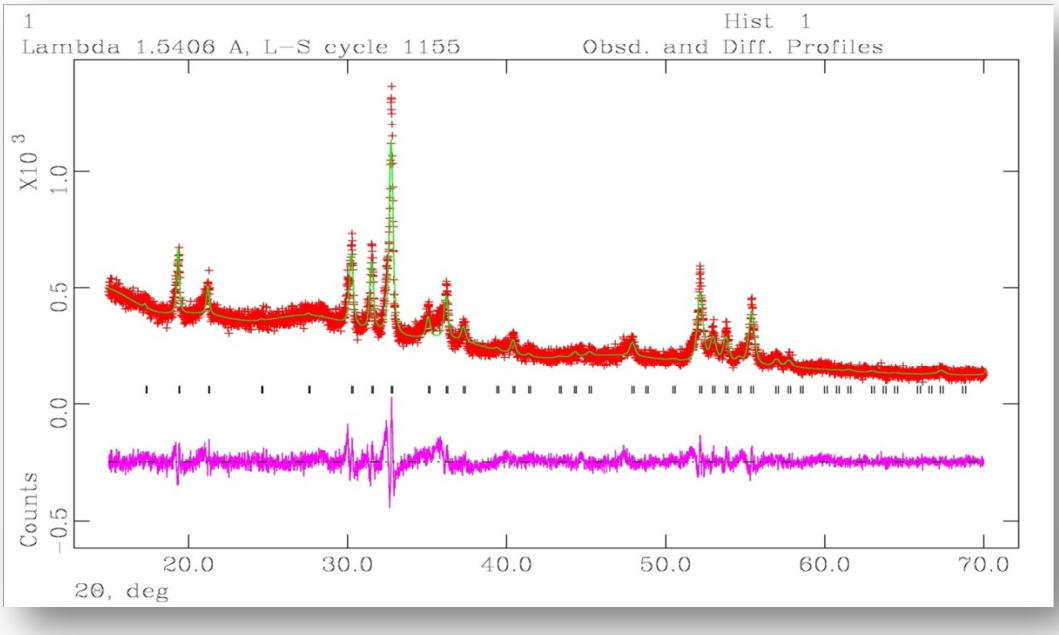

Figure 4.1 Observed (red crosses), calculated (green curve), and difference (purple curve) powder X-ray diffraction patterns for microcrystalline $Na_8Ge_3Si_{38}$. Black tick marks (lower) indicate reflection positions for the $Na_8Ge_3Si_{38}$ phase.

The composition with a stoichiometry of $Na_8Ge_3Si_{38}$ was obtained from the refinement of powder XRD data collected on the microcrystalline clathrate-I specimen, respectively (Table 4.1).

Table 4.1. Crystallographic data and refined atomic positions and isotropic atomic displacement parameters from the powder specimens of the clathrate-I phase.

	$Na_8Ge_3Si_{38}$
Formula weight	1441.06
space group	$Pm\bar{3}n$
a, Å	10.2207
V, $Å^3$	1067.69
D_{calc} , gcm^{-3}	2.241
$\chi 2$	1.564
Rp	0.0620
Rwp	0.0823
U_{iso} (Na1)	0.0363
U_{iso} (Na2)	0.0271
U_{iso} (Si3)	0.0137
Occupancy (Si3)	1.0
x (Si3)	0.3088
y (Si3)	0.1173
U_{iso} (Si2)	0.0101
Occupancy (Si2)	0.8786
z (Si2)	0.1847
U_{iso} (Ge1)	0.0059
Occupancy (Ge1)	0.4322
x (Ge1)	0.5
z (Ge1)	0

$Na_8Ge_3Si_{38}$ atom positions: Na1, *2a* 0, 0,0; Na2, *6d* 1/2, 0, 1/4;
Ge1, *6c* x, 1/4, z ; Si2, *16i* z, z, z; Si3, *24k* x, y, 0

The crystal structure of the type I $Na_8Ge_3Si_{38}$ clathrate is of cubic phase with space group $Pm\bar{3}n$. The guest sodium atoms are fully occupied in the *2a* and *6d*

crystallographic sites. The Si and Ge atoms compose the framework atoms with the Si atoms fully occupying the *24k* crystallographic site and the Si and Ge partially occupying the *6c* and *16i* crystallographic sites.

The synthesis of the new type I clathrate, $Na_8Ge_3Si_{38}$, was achieved through the novel SPS method. This is the first time that the type I clathrate, $Na_8Ge_3Si_{38}$ has been synthesized. SiGe clathrates are of great interest for optoelectronic applications and this research will expand the fundamental knowledge needed to create type I and II SiGe clathrates. This research also demonstrates the enormous potential that the new SPS synthesis technique has in creating novel materials such as inorganic clathrates.

5. Synthesis of single crystal $Ba_2Cs_6Ga_8Sn_{38}$ by flux method

5.1. History of flux synthesis for clathrates

High temperature materials synthesis has long been a method of producing inorganic materials. One method that has commonly been used is through high temperature solid state synthetic reactions [65]. This "flux" method was employed by Nolas et al. [66,67,68] to grow single crystals of type I Sn clathrates and single crystals of type I $(Sr,Eu)_8Ga_{16}Ge_{30}$ clathrates , by Chakoumakos et al. [69] to grow single crystals of $Sr_8Ga_{16}Ge_{30}$, by Tanaka et al.[70] to grow single crystals of the type I $K_8Ga_8Sn_{38}$ clathrate, and more recently by Mano et al.[22] to grow single crystals of the type II clathrates $(K,Ba)_{24}(Ga,Sn)_{136}$. This synthesis method was also used by Suekini et al. [71] to grow single crystals of type I $Ba_8Ga_{16}Sn_{30}$. That experiment was replicated for reference (Fig 5.1). Avila et al. [72] and Saiga et al. [73] have characterized this clathrate and found it to have potential for thermoelectric applications. Using this "flux" method, this laboratory has synthesized single crystals of the novel type I clathrate, $Ba_2Cs_6Ga_8Sn_{38}$.

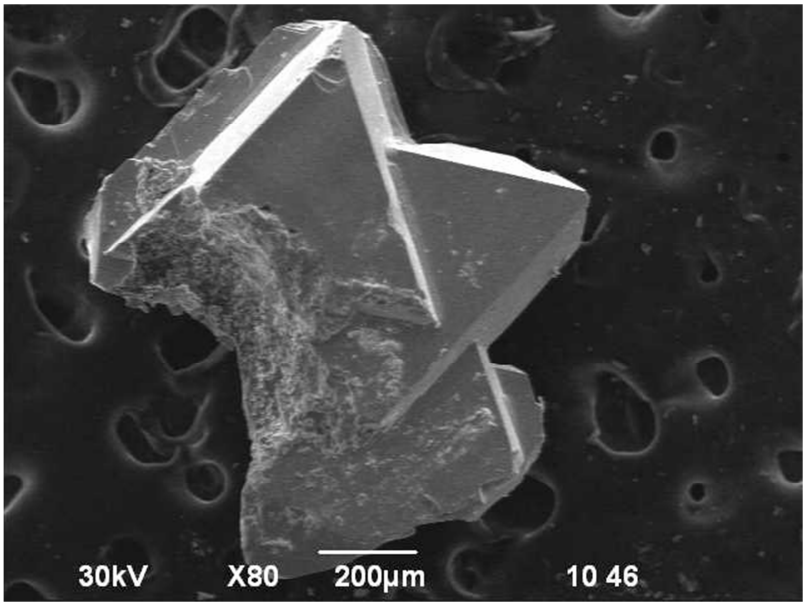

Figure 5.1: SEM image of the single crystals of type I clathrate $Ba_8Ga_{16}Sn_{30}$.

5.2. *Experimental procedure*

The single crystal $Ba_2Cs_6Ga_8Sn_{38}$ was grown by the "flux" method using excess Sn as the flux. The starting compositions for the four elements had a molecular ratio of Ba:8, Cs:16, Ga:47, and Sn:96, (Alfa Aesar, 99.99%) and were then loaded with that molecule ratio into a tungsten crucible which was then sealed inside a stainless steel canister under nitrogen (Figure 5.2).

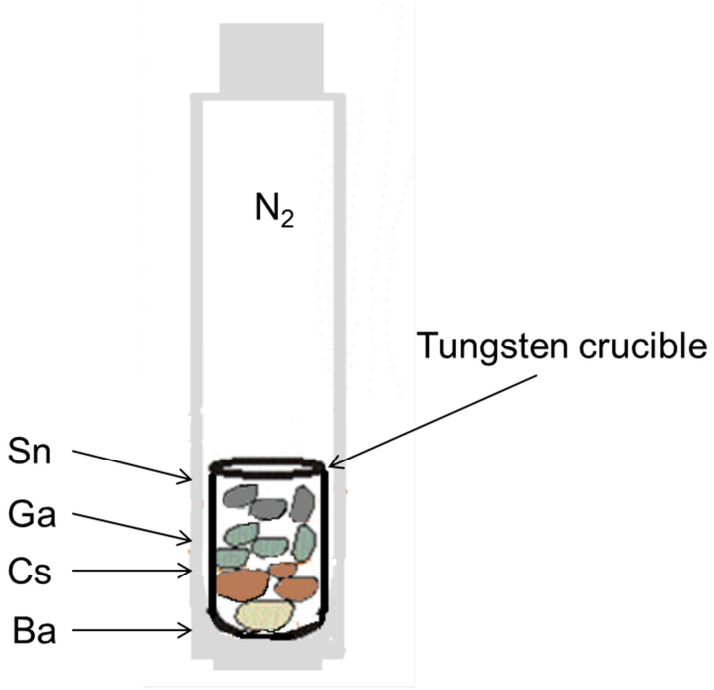

Fig 5.2: Experimental setup for self-flux method

This canister was sealed in a quartz tube under nitrogen and reacted at 550 ^{o}C for 15 hours. It was then cooled at a rate of 1 ^{o}C/hr to a temperature of 450 ^{o}C. Finally, at this temperature, the quartz tube was quickly removed from the furnace and air quenched in a sand bath. The canister was opened in air under normal laboratory conditions. The single crystals of the type I clathrate (see Figure 5.3) were picked out from the resulting flux product. The single crystals were than imaged by a SEM and were collected using a JEOL JSM-6390LV and EDS data were collected using an Oxford INCA X-Sight 7582M. Single-crystal XRD data of the $Ba_2Cs_6Ga_8Sn_{38}$ crystals were obtained at 293 K on a STOE diffractometer using a graphite monochromator and a Mo K_α fine-focus sealed tube with a wavelength of 0.71073 Å at the University of California-Davis. Structural refinements were performed using SHELXL-97 (Tables 5.1 – 5.3).

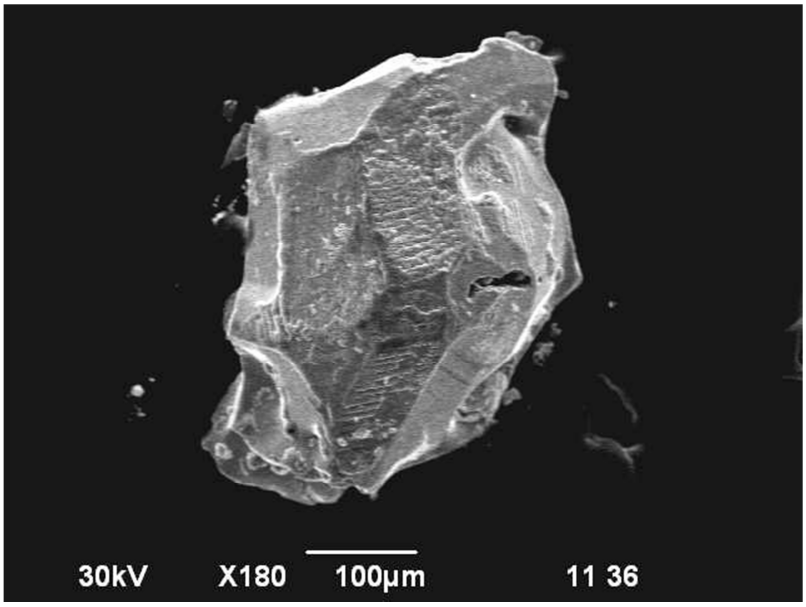

Fig 5.3: An SEM image of the new type I clathrate, $Ba_2Cs_6Ga_8Sn_{38}$

5.3. *Crystal structure*

The composition with a stoichiometry of $Ba_2Cs_6Ga_8Sn_{38}$ was obtained from the refinement of the single-crystal XRD data (Tables 5.1-5.3). The crystal structure of the type I $Ba_2Cs_6Ga_8Sn_{38}$ clathrate is of cubic phase with space group $Pm\bar{3}n$. The Ba and Cs atoms are the guest atoms in the framework and are fully occupied with the Ba atoms in the *2a* crystallographic site and the Cs atoms in the *6d* crystallographic site. The Ga and Sn atoms compose the framework atoms with the Ga and Sn atoms each partially occupying the *16i*, *24k*, and *6c* crystallographic sites (Table 5.2).

Table 5.1. Single-crystal XRD refinement data for $Ba_2Cs_6Ga_8Sn_{38}$

Composition	$Ba_2Cs_6Ga_8Sn_{38}$
Formula weight	5953.10
Crystallinity	single-crystal
Crystal size (mm)	0.25
Crystal system, space group	Cubic, $Pm\bar{3}n$
Lattice parameter, *a*/Å	11.994(4)
Calculated density / gcm^{-3}	3.450
2θ (deg.)	4.90 to 38.07
R	0.0144
wR	0.0297
Goodnes of fit on χ^2	1.477

Table 5.2. Refined atomic positions, occupancies, and isotropic atomic displacement parameters (U_{iso}) for microcrystalline $Ba_2Cs_6Ga_8Sn_{38}$.

Atom	***x/a***	***y/a***	***z/a***	**Occ.**	**U_{iso} (Å)**
Ba1	0	0	0	1	0.0072
Cs2	0.5	0	0.25	1	0.0142
Ga1	0.31059	0.11825	0	0.15	0.0082
Sn1	0.31059	0.11825	0	0.85	0.0082
Ga2	0.18378	0.18378	0.18378	0.10	0.0075
Sn2	0.18378	0.18378	0.18378	0.90	0.0075
Ga3	0.5	0.25	0	0.37	0.0092
Sn3	0.5	0.25	0	0.63	0.0092

Table 5.3. Refined anisotropic atomic displacement parameters (U_{ij}/Å) for microcrystalline $Ba_2Cs_6Ga_8Sn_{38}$.

Atom	U_{11}	U_{22}	U_{33}	U_{12}	U_{13}	U_{23}
Ba1	0.00716	0.00716	0.00716	0	0	0
Cs2	0.01743	0.01743	0.00779	0	0	0
Ga1	0.00842	0.00856	0.00758	0.00045	0	0
Sn1	0.00842	0.00856	0.00758	0.00045	0	0
Ga2	0.00751	0.00751	0.00751	-0.00039	-0.00039	-0.00039
Sn2	0.00751	0.00751	0.00751	-0.00039	-0.00039	-0.00039
Ga3	0.00897	0.00950	0.00897	0	0	0
Sn3	0.00897	0.00950	0.00897	0	0	0

The new type I clathrate, $Ba_2Cs_6Ga_8Sn_{38}$, was synthesized using the solid state "flux" synthesis technique. The crystal structure of this new clathrate was investigated. Due to the previous studies of Avila et al. [72] and Saiga et al. [73] in showing the type I $Ba_8Ga_{16}Ge_{30}$ clathrate being a good thermoelectric material, this new $Ba_2Cs_6Ga_8Sn_{38}$ type I clathrate should be further characterized and analyzed to determine if this is also a good thermoelectric material.

6. **Summary and Future directions**

In the process of obtaining my Masters of Science degree a lot has been accomplished. SPS was used to selectively synthesize microcrystalline and single crystal type I Na_8Si_{46} and type II $Na_{24}Si_{136}$ clathrates by varying the temperature and pressure. The ionic liquid synthesis method was used to selectively synthesize the type I and II clathrates, Na_8Si_{46} and $Na_{24}Si_{136}$ respectively, by varying the reaction time and temperature. Two new type I clathrates were created, $Na_8Ge_3Si_{38}$ and $Ba_2Cs_6Ga_8Sn_{38}$ via the SPS and "flux" synthesis techniques, respectively. The crystal structure of each clathrate was investigated by XRD and EDS.

Although much has been done in this study regarding the synthesis and investigations of type I and II clathrates of group 14, there is much to do in the future that can build on this research. The characterization of the new type I clathrates, $Na_8Ge_3Si_{38}$ and $Ba_2Cs_6Ga_8Sn_{38}$, in order to determine their physical properties is of interest. This study also shows the potential of creating a new type I clathrate $Na_8Ge_xSi_y$ with varying Ge content via SPS. Finally, this study demonstrates the potential to make a type II Si_xGe_y clathrate by using the ionic liquid synthesis method (as of now the ionic liquid method has been the only synthesis technique to produce type II Ge clathrates[54,21]). There is much to do involving clathrate research in moving forward, allowing one to further understand the fundamental physics and chemistry of clathrates, and use that knowledge to determine and vary their physical properties for a variety of applications.

7. References

[1] G. S. Nolas; G. A. Slack; S. B. Schujman, in *Semiconductors & Semimetals*, edited by T. M. Tritt (Academic Press, San Diego, 2000), Vol. 69, p. 255.

[2] G. S. Nolas, J. L. Cohn, G. A. Slack, and S. B. Schujman, Appl Phys Lett **73** (2), 178 (1998).

[3] J. L. Cohn, G. S. Nolas, V. Fessatidis, T. H. Metcalf, and G. A. Slack, Phys Rev Lett **82** (4), 779 (1999).

[4] K. Moriguchi, S. Munetoh, and A. Shintani, Phys Rev B **62** (11), 7138 (2000).

[5] J. Gryko, P. F. McMillan, R. F. Marzke, G. K. Ramachandran, D. Patton, S. K. Deb, and O. F. Sankey, Phys Rev B **62** (12), R7707 (2000).

[6] X. Blase, P. Gillet, A. San Miguel, and P. Melinon, Phys Rev Lett **93** (23) (2004).

[7] M. H. Phan, G. T. Woods, A. Chaturvedi, S. Stefanoski, G. S. Nolas, and H. Srikanth, Appl Phys Lett **93** (25) (2008).

[8] S. Paschen, W. Carrillo-Cabrera, A. Bentien, V. H. Tran, M. Baenitz, Y. Grin, and F. Steglich, Phys Rev B **64** (21), art. no. (2001).

[9] K. A. Kovnir and A. V. Shevelkov, Usp Khim+ **73** (9), 999 (2004).

[10] J. S. Kasper, Hagenmul.P, M. Pouchard, and C. Cros, Science **150** (3704), 1713 (1965).

[11] C. Cros; M. Pouchard; P. Hagenmuller, J Solid State Chem **2**, 570 (1970).

[12] G. K. Ramachandran, J. J. Dong, J. Diefenbacher, J. Gryko, R. F. Marzke, O. F. Sankey, and P. F. McMillan, J Solid State Chem **145** (2), 716 (1999).

[13] M. Beekman and G. S. Nolas, Physica B **383** (1), 111 (2006).

[14] S. Stefanoski, L. N. Reshetova, A. V. Shevelkov, and G. S. Nolas, J Electron Mater **38** (7), 985 (2009).

[15] S. Bobev and S. C. Sevov, J Solid State Chem **153** (1), 92 (2000).

[16] M. Beekman and G. S. Nolas, J Mater Chem **18** (8), 842 (2008).

[17] P. Rogl, edited by D. M. Rowe (CRC Press, Boca Raton, 2005).

[18] M O'Keeffe, GB Adams, and OF Sankey, Philosophical Magazine Letters **78** (1), 21 (1998).

[19] M Pouchard, C Cros, P Hagenmuller, E Reny, A Ammar, M Menetrier, and JM Bassat, Solid State Sci **4** (5), 723 (2002).

[20] M Beekman, JA Kaduk, J Gryko, W Wong-Ng, A Shapiro, and GS Nolas, J Alloy Compd **470** (1-2), 365 (2009).

[21] A. M. Guloy, Z. J. Tang, R. Ramlau, B. Bohme, M. Baitinger, and Y. Grin, Eur J Inorg Chem (17), 2455 (2009).

[22] S Mano, T Onimaru, S Yamanaka, and T Takabatake, Phys Rev B **84** (21) (2011).

[23] Y Mudryk, P Rogl, C Paul, S Berger, E Bauer, G Hilscher, C Godart, and H Noel, J Phys-Condens Mat **14** (34), 7991 (2002).

[24] M. Beekman, E. N. Nenghabi, K. Biswas, C. W. Myles, M. Baitinger, Y. Grin, and G. S. Nolas, Inorg Chem **49** (12), 5338 (2010).

[25] J. Gryko, United States Patent No. (6,423,286).

[26] S. Stefanoski, C. D. Malliakas, M. G. Kanatzidis, and G. S. Nolas, Inorg Chem **51** (16), 8686 (2012).

[27] GS Nolas, DG Vanderveer, AP Wilkinson, and JL Cohn, J Appl Phys **91** (11), 8970 (2002).

[28] G. A. Slack, in *CRC Handbook of Thermoelectrics*, edited by D. M. Rowe (CRC Press, Boca Raton, 1995).
[29] GJ Snyder and ES Toberer, Nat Mater **7** (2), 105 (2008).
[30] H. Morkoc, S. Strite, G. B. Gao, M. E. Lin, B. Sverdlov, and M. Burns, J Appl Phys **76** (3), 1363 (1994).
[31] LT CANHAM, Appl Phys Lett **57** (10), 1046 (1990).
[32] L. L. Kazmerski, J. Electron Spectrosc. Relat. Phenom. **150** (2-3), 105 (2006).
[33] GB ADAMS, M OKEEFFE, AA DEMKOV, OF SANKEY, and YM HUANG, Phys Rev B **49** (12), 8048 (1994).
[34] H. V. Atkinson and S. Davies, Metall Mater Trans A **31** (12), 2981 (2000).
[35] M. Tokita, Journal Society of Powder Technology of Japan **30**, 790 (1993).
[36] Z. A. Munir, U. Anselmi-Tamburini, and M. Ohyanagi, J Mater Sci **41** (3), 763 (2006).
[37] J. Schmidt, M. Boehling, U. Burkhardt, and Y. Grin, Sci Technol Adv Mat **8** (5), 376 (2007).
[38] M. Omori, Mat Sci Eng a-Struct **287** (2), 183 (2000).
[39] J. Galy, M. Dolle, T. Hungria, P. Rozier, and J. P. Monchoux, Solid State Sci **10** (8), 976 (2008).
[40] M. Nygren and Z. J. Shen, Solid State Sci **5** (1), 125 (2003).
[41] M. Beekman, M. Baitinger, H. Borrmann, W. Schnelle, K. Meier, G. S. Nolas, and Y. Grin, J Am Chem Soc **131** (28), 9642 (2009).
[42] S. Stefanoski, M. Beekman, W. Wong-Ng, P. Zavalij, and G. S. Nolas, Chem Mater **23** (6), 1491 (2011).
[43] H. O. Horie, T. Kikudome, K. Teramura, and S. Yamanaka, J Solid State Chem **182** (1), 129 (2009).
[44] E. Reny, P. Gravereau, C. Cros, and M. Pouchard, J Mater Chem **8** (12), 2839 (1998).
[45] M. Beekman, W. Schnelle, H. Borrmann, M. Baitinger, Y. Grin, and G. S. Nolas, Phys Rev Lett **104** (1) (2010).
[46] P. Scherrer, Nachrichten von der Gesellschaft der Wissenschaften zu Göttingen, Mathematisch-Physikalische Klasse **26**, 98 (1918).
[47] J. I. Langford and A. J. C. Wilson, J Appl Crystallogr **11** (Apr), 102 (1978).
[48] T. M. Atkins, A. Y. Louie, and S. M. Kauzlarich, Nanotechnology **23** (29) (2012).
[49] J. H. Park, L. Gu, G. von Maltzahn, E. Ruoslahti, S. N. Bhatia, and M. J. Sailor, Nat Mater **8** (4), 331 (2009).
[50] M. J. Earle and K. R. Seddon, Pure Appl Chem **72** (7), 1391 (2000).
[51] J. S. Wilkes, Green Chem **4** (2), 73 (2002).
[52] C. L. Hussey, Pure Appl Chem **60** (12), 1763 (1988).
[53] Z. Ma, J. H. Yu, and S. Dai, Adv Mater **22** (2), 261 (2010).
[54] A. M. Guloy, R. Ramlau, Z. J. Tang, W. Schnelle, M. Baitinger, and Y. Grin, Nature **443** (7109), 320 (2006).
[55] B. Bohme, S. Hoffmann, M. Baitinger, and Y. Grin, Z Naturforsch B **66** (3), 230 (2011).
[56] B. Bohme, A. Guloy, Z. J. Tang, W. Schnelle, U. Burkhardt, M. Baitinger, and Y. Grin, J Am Chem Soc **129** (17), 5348 (2007).
[57] B. Bohme, U. Aydemir, A. Ormeci, W. Schnelle, M. Baitinger, and Y. Grin, Sci Technol Adv Mat **8** (5), 410 (2007).
[58] Y. Liang, B. Bohme, M. Reibold, W. Schnelle, U. Schwarz, M. Baitinger, H. Lichte, and Y. Grin, Inorg Chem **50** (10), 4523 (2011).
[59] S. Yamanaka, E. Enishi, H. Fukuoka, and M. Yasukawa, Inorg Chem **39** (1), 56 (2000).
[60] A. C. Larson; R. B. Von Dreele, 2004.

[61] B. H. Toby, J Appl Crystallogr **34**, 210 (2001).
[62] G. S. Nolas and G. A. Slack, Am Sci **89** (2), 136 (2001).
[63] M. Beekman, S. Stefanoski, W. Wong-Ng, J. A. Kaduk, Q. Huang, C. Reeg, C. R. Bowers, and G. S. Nolas, J Solid State Chem **183** (6), 1272 (2010).
[64] S. Stefanoski; M. C. Blosser; G. S. Nolas, Cryst Growth Des **13**, 195 (2013).
[65] R. Xu; Q. Su, edited by Ruren Xu; Wenqin Pang; and Qisheng Huo (Elsevier B.V., 2011).
[66] G. S. Nolas, T. J. R. Weakley, and J. L. Cohn, Chem Mater **11** (9), 2470 (1999).
[67] G. S. Nolas, B. C. Chakoumakos, B. Mahieu, G. J. Long, and T. J. R. Weakley, Chem Mater **12** (7) (2000).
[68] G. S. Nolas, T. J. R. Weakley, J. L. Cohn, and R. Sharma, Phys Rev B **61** (6), 3845 (2000).
[69] B. C. Chakoumakos, B. C. Sales, D. G. Mandrus, and G. S. Nolas, J Alloy Compd **296** (1-2), 80 (2000).
[70] T. Tanaka, T. Onimaru, K. Suekuni, S. Mano, H. Fukuoka, S. Yamanaka, and T. Takabatake, Phys Rev B **81** (16) (2010).
[71] K. Suekuni, M. A. Avila, K. Umeo, H. Fukuoka, S. Yamanaka, T. Nakagawa, and T. Takabatake, Phys Rev B **77** (23) (2008).
[72] M. A. Avila, K. Suekuni, K. Umeo, H. Fukuoka, S. Yamanaka, and T. Takabatake, Appl Phys Lett **92** (4) (2008).
[73] Y. Saiga, K. Suekuni, B. Du, and T. Takabatake, Solid State Communications **152** (20), 1902 (2012).